ACI STRUCTURAL JOURNAL TECHNICAL PAPER

Title no. 99-S22

Experimental Studies on Full-Scale High-Strength Concrete Columns

by Yan Xiao and Henry W. Yun

Six full-scale high-strength concrete columns with compressive strengths of approximately 63 MPa were tested under cyclic lateral force and a constant axial load equal to 20 to 34% of the column's axial load capacity. The 510 x 510 mm square columns were reinforced with four No. 29 (ASTM No. 9) and four No. 36 (ASTM No. 11) bars constituting a longitudinal steel ratio of 2.6% of the column cross-sectional area. The main experimental parameters were the transverse reinforcement detail and the axial load level. It was found that the hysteretic behavior and ultimate deformability of high-strength concrete columns were significantly influenced by the amount and details of transverse reinforcement in the potential plastic hinge regions as well as by the axial load level. Excellent hysteretic behavior that achieved a drift ratio of 6% without degradation of the load-carrying capacity was developed by columns with a transverse reinforcement not less than 82% of that specified in the seismic design provisions of ACI 318-99, when the axial load ratio was 20%. Similar columns, however, only achieved an ultimate drift ratio of 3% when the axial load was above 30% of the column's axial load capacity. For the same transverse reinforcement configuration and testing condition, improved behavior was observed for the model column with higher-strength transverse reinforcement.

Keywords: column; ductility; flexural strength; high-strength concrete.

INTRODUCTION

The use of high-strength concrete (HSC) in tall buildings can offer many advantages compared with normal-strength concrete (NSC). HSC structural columns are particularly prominent for the possibilities of increased load-carrying capacities and stiffness. Such capacity or stiffness enhancement may result in reduced column size and increased floor space compared with NSC structures. Exploring the merits of using HSC in earthquake-resistant tall buildings, however, needs special precautions to ensure the ductility of the structural components made of HSC. Due to insufficient research for the development of seismic design guidelines, the application of HSC in lateral load-resisting systems has been extremely limited in regions of high seismicity in the U.S., such as southern California. This study is part of a comprehensive research program aimed at developing design provisions for the use of HSC in regions of high seismicity. Its ultimate goal is to evaluate confinement requirements to ensure ductile behavior of HSC columns utilized in lateral load-resisting frames.

Although an increasing amount of research[1-6] on the seismic behavior of HSC columns is becoming available, tests on full-scale HSC columns are scarce. Full-scale testing of HSC columns requires large-capacity loading facilities. In particular, the force required to simulate a realistic axial load level of HSC columns in tall buildings is significantly large, making testing more difficult and costly. A new testing facility recently developed by the authors at the University of Southern California enables full-scale experimental testing on structural columns. This paper presents the experimental results on six full-scale HSC columns subjected to simulated seismic loading.

RESEARCH SIGNIFICANCE

Due to insufficient research, the advantages of HSC have not been fully explored as to the design and construction of tall buildings in seismic regions. Many existing studies of HSC columns are based on relatively small-size specimens due to the high level of loads required in testing full- or near full-size columns. A simple and efficient method for testing large- to full-scale columns with simulated seismic loads is presented in the paper. The method enables the experimental study of full-scale high-strength concrete columns with a 510 x 510 mm square section subjected to cyclic lateral force and constant axial load. The test results not only fill the gap of full-scale test data, but also contribute to the future development of design guidelines for earthquake resistant high-strength concrete structures. In addition, the full-scale column test data can be used for calibration of analytical tools.

EXPERIMENTAL PROGRAM

Specimen design

Six full-scale column specimens were designed to simulate typical columns of multistory buildings in seismic regions. The testing matrix is shown in Table 1, and the specimen details are illustrated in Fig. 1. The columns were 510 x 510 mm (20 x 20 in.) square in cross section with a height of 1778 mm (70 in.) from the point of lateral loading to the top of the footing. The columns were reinforced with four No. 36 (ASTM No. 11, nominal diameter = 35.8 mm = 1.41 in.) bars plus four No. 29 (ASTM No. 9, nominal diameter = 28.7 mm = 1.128 in.) bars, constituting a longitudinal reinforcement ratio of 2.6%. The main testing parameters were the transverse reinforcement details and the axial load level.

In the seismic design provisions of ACI 318-99,[7] the cross-sectional area of transverse reinforcement for the potential plastic hinge region of a column is specified by the following equations

$$A_{sh} \geq 0.3\frac{sh_c f'_c}{f_{yh}}\left(\frac{A_g}{A_{ch}} - 1\right) \quad (1a)$$

ACI Structural Journal, V. 99, No. 2, March-April 2002.
MS No. 01-177 received June 1, 2001, and reviewed under Institute publication policies. Pertinent discussion will be published in the January-February 2003 *ACI Structural Journal* if received by September 1, 2002.

ACI member **Yan Xiao** *is an associate professor of civil engineering at the University of Southern California, Los Angeles, Calif. He received his bachelor of engineering from Tianjin University, China, in 1982, and his MS and PhD from Kyushu University, Japan, in 1986 and 1989, respectively. His research interests include earthquake-resistant design of structures, structural concrete, steel, hybrid, and composite systems, and structural materials. He is a member of ACI-ASCE Committees 441, Reinforced Concrete Columns; and 335, Composite and Hybrid Structures.*

Henry W. Yun *is a PhD candidate in civil engineering at the University of Southern California. He received his BS from the University of California, Davis, Calif., and his MS from the University of Southern California. His research interests include earthquake-resistant design of reinforced concrete structures.*

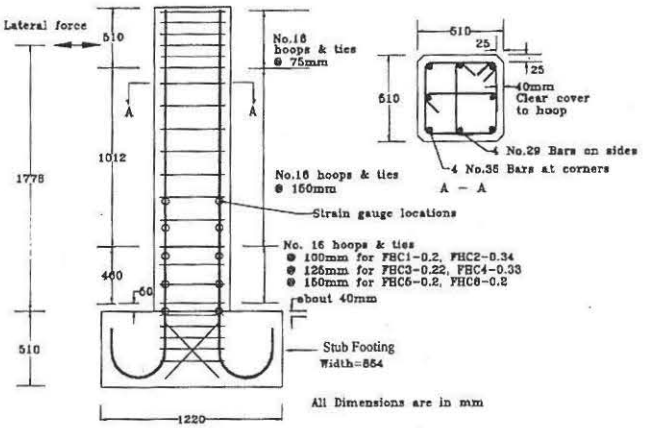

Fig. 1—Details of full-scale column specimens.

or

$$A_{sh} \geq 0.09 s h_c \frac{f_c'}{f_{yh}} \quad (1b)$$

where A_{sh} is the total transverse steel cross-sectional area within the spacing s; h_c is the cross-sectional dimension of the column core measured center-to-center of the outermost peripheral hoops; f_c' is the specified compressive strength of concrete; f_{yh} is the specified yield strength of the transverse reinforcement; A_g is the gross area of the column section; and A_{ch} is the cross-sectional area of a column measured out-to-out of transverse reinforcement. It should be pointed out that, in the following discussions and analysis, all specified material strengths per design codes are replaced by using the actual strengths obtained from material tests. This was to reflect the research purpose of evaluating the adequacy of various design equations through actual testing, rather than providing safety factors for design. In earlier versions of the ACI 318 code, the hoop spacing is limited to 1/4 of the minimum dimension of the column or 100 mm (4 in.), whichever is smaller. The hoop spacing in the ACI 318-99 code, however, is changed to not exceeding: 1/4 of the minimum dimension of the member; six times the diameter of the longitudinal reinforcement; and s_x, given as

$$s_x = 4 + \left(\frac{14 - h_x}{3}\right) \quad (2)$$

where h_x is the maximum horizontal spacing of hoop or crosstie legs on the faces of the column, and both s_x and h_x are measured in inches. This change relaxed the requirements

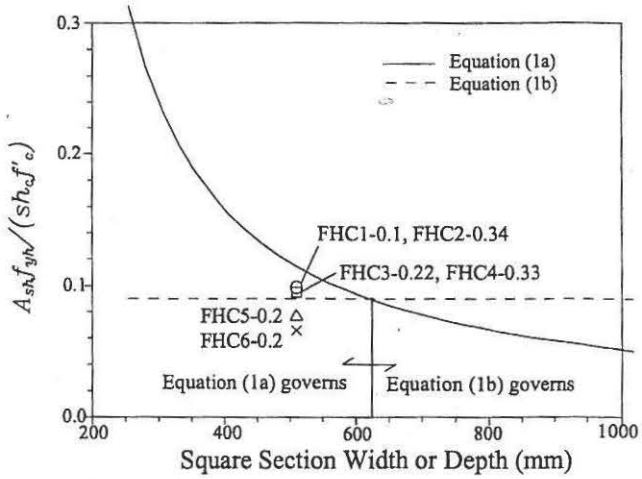

Fig. 2—Comparison of transverse confinement indexes of model columns with code requirements.

of the transverse reinforcement spacing in the potential plastic hinge region up to 150 mm (6 in.).

Figure 2 compares the predictions using Eq. (1(a)) and (b) for square columns with a constant cover thickness of 38 mm (1.5 in.). The vertical axis shows the confinement index, which is defined as the total transverse steel area A_{sh}, within the spacing s, divided by $sh_c f_c'/f_{yh}$, while the horizontal axis shows the width or depth of square columns. As is evident from Fig. 2, Eq. (1(a)) governs the design of square columns with a side dimension less than approximately 610 mm (24 in.), while Eq. (1(b)) controls the design for larger depths. The relative values of the transverse reinforcement for the hinge regions of the six full-scale model columns based on actual material strengths are also plotted in Fig. 2. For the selected dimension of the specimens tested in this research, Eq. (1(a)) governs the determination of A_{sh}.

Model Columns FHC1-0.2 and FHC2-0.34 were transversely reinforced with No. 16 (ASTM No. 5, nominal diameter = 15.9 mm = 5/8 in.) hoops and cross ties spaced at 100 mm (4 in.) in the potential plastic hinge region with a length of 510 mm (20 in.) at the column end. The transverse reinforcements were spaced at 150 mm (6 in.) outside the plastic hinge region. The transverse reinforcement in the potential plastic hinge regions of these two specimens provided approximately 86% of the required confinement steel based on Eq. (1(a)) and actual material strengths. The spacing of the transverse reinforcement was more stringent than the ACI 318-99 requirements, since the specimens were designed prior to the implementation of the relaxed spacing requirement.

In Specimens FHC3-0.22 and FHC4-0.33, the spacing of the No. 16 transverse reinforcement in the potential plastic hinge regions was increased to 125 mm (5 in.). This spacing satisfied the requirements of ACI 318-99, which relaxed the maximum spacing requirement for transverse reinforcement from 100 to 150 mm (4 to 6 in.). Due to the use of higher-strength transverse reinforcement in these two columns, the amount of transverse reinforcement was approximately 82% of that required by Eq. (1), and is comparatively close to that of Specimens FHC1-0.2 and FHC2-0.34.

Specimen FHC5-0.2 was reinforced with No. 16 hoops and ties spaced at 150 mm (6 in.). This was at the limit allowed by the ACI 318-99 code. Consequently, FHC5-0.2 had approximately 57% of the confinement required by Eq. (1(a)).

Table 1—Testing matrix

Specimen	Longitudinal steel	Transverse steel for column potential plastic hinge region	Concrete strength f_c', MPa	Concrete strength f_c', MPa*	Axial load ratio $P/A_g f_c'$ (axial load)
FHC1-0.2	4 No. 29 and 4 No. 36 (f_y = 473 MPa)	No. 16 hoops and ties at 100 mm (f_y = 445 MPa)	64.1	—	0.20 (3334 kN)
FHC2-0.34		No. 16 hoops and ties at 100 mm (f_y = 445 MPa)	62.1	75.5*	0.34 (5373 kN)
FHC3-0.22		No. 16 hoops and ties at 125 mm (f_y = 524 MPa)	62.1	75.5*	0.22 (3630 kN)
FHC4-0.33		No. 16 hoops and ties at 125 mm (f_y = 525 MPa)	62.1	75.5*	0.33 (5240 kN)
FHC5-0.2		No. 16 hoops and ties at 150 mm (f_y = 445 MPa)	64.1	—	0.20 (3334 kN)
FHC6-0.2		No. 16 hoops and ties at 150 mm (f_y = 524 MPa)	64.1	—	0.20 (3334 kN)

*f_c' = concrete strength obtained from water-cured standard cylinder specimens.
Note: 1) Specimen name designation example: FHC1-0.2 represents high-strength concrete full-scale flexural testing model column No. 1 with axial load of 0.2; 2) concrete strength f_c' based on average strength of three 152 x 305 mm (6 x 12 in.) cylinders cured in air-dry condition; 3) axial load ratio = $P/(A_g f_c')$; and 4) nominal diameter = 28.7 mm (1.128 in.) for No. 29 (No. 9) bars, 35.8 mm (1.41 in.) for No. 36 (No. 11) bars, and 15.9 mm (0.625 in.) for No. 16 (No. 5) bars.

Higher-strength steel was used in the transverse reinforcement for model Column FHC6-0.2. In this specimen, the hoops and ties were spaced at 150 mm (6 in.). The total cross-sectional area of transverse reinforcement was approximately equal to 68% of the value given by Eq. (1(a)).

All of the hoops and ties satisfied the detailing requirements of ACI 318-99. Each set of transverse reinforcement consisted of a peripheral hoop with 135-degree hooks and a pair of cross ties with a 135-degree hook at one end and a 90-degree hook at the other end. The 90-degree hooks were alternated for the cross ties throughout the height of the column.

The specimens were designed and constructed with a stiff stub footing of 1219 x 864 x 508 mm (48 x 34 x 20 in.). The stub footings were heavily reinforced to eliminate any premature failure during testing.

Specimen construction

Construction of the specimens was carried out at the Structural Laboratory of the University of Southern California. The six columns were divided into two groups with three specimens in each group. Column stubs were cast first and cured for more than 1 week before the column forms were set up. Casting of column concrete also took place in the laboratory with HSC that was supplied by a local concrete plant. The specimens were kept in the forms for 2 weeks after casting. The forms were then removed and the specimens cured in air-dry conditions until testing.

Material properties

Material properties for all specimens are summarized in Table 1. The mixture proportions per m^3 of HSC were 187 kg water; 415 kg cement; 148 kg Class-F fly ash; 45 kg silica fume; 868 kg coarse aggregates; and 710 kg fine aggregates. The water-cementitious materials ratio (*w/cm*) was 0.30. High-range water-reducing admixture was also used to improve workability and setting time. The average slump at casting was approximately 150 mm (6 in.). It should be pointed out that the mixture proportions were determined based on extensive trial mixtures[8] using materials available to southern California, which is one of the regions of highest seismicity in the U.S. The compressive strength based on this mixture proportion design approximately doubles the typical upper strength of 34.5 MPa (5000 psi) for general use in seismic-resisting elements in southern California.

The concrete compressive strength values shown in Table 1 are based on compression tests on concrete cylinders that were 150 mm in diameter and 300 mm in height. The cylinders were prepared and cured at the site of construction of the test specimens. Compressive strength values obtained from water-cured cylinders were approximately 20% higher than those from air-cured cylinders. In this study, it was assumed that the concrete strength obtained from the air-cured cylinders represented more closely the actual concrete strength of the column specimens.

Grade 420 (ASTM A615 Grade 60) steel with an average yield strength of 469 MPa (68 ksi) was used for longitudinal reinforcing bars in all of the columns. Three specimens were transversely reinforced with Grade 420 steel with an average yield strength of 445 MPa (64.5 ksi). The other three specimens had Grade 520 (ASTM Grade 75) bars for transverse reinforcement with an average yield strength of 524 MPa (76 ksi).

Test setup

A loading system that enables the full-scale testing of high-strength concrete columns was recently developed by the authors. The stub footing of the specimen was post-tensioned to a stiff steel-concrete composite reaction beam. The reaction beam is 1.2 m wide and 5 m long, and is anchored to a deep concrete foundation. As shown in Fig. 3(a), the testing system utilizes two actuators with a 1334 kN (300 kip) capacity for cyclic loading in both lateral and axial directions. An axial force as large as 6200 kN (approximately 1400 kips) can be applied to the specimen through a specially-designed lever arm that amplifies the force output of the vertical actuator by six times. Figure 3(b) schematically illustrates the concept of the lever arm system for axial loading. By setting the distance between the axis of the vertical connectors and the column axis equal to 1/5 of that between the vertical actuator and the column axis, an axial load of six times the actuator force can be applied to the specimen.

As shown in Fig. 3(b), if a lateral displacement Δ is induced, the applied axial load becomes inclined; thus, the true vertical load subjected by the column is the vertical component of the

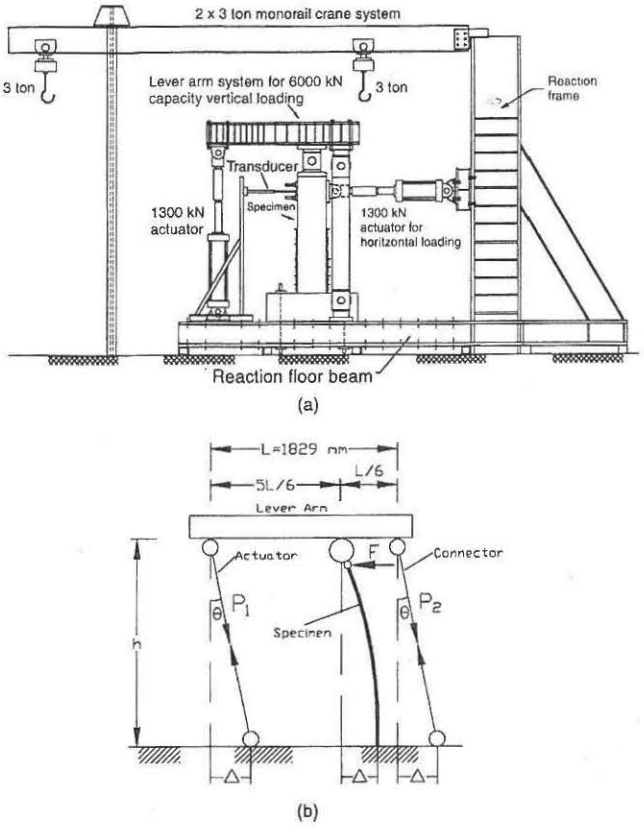

Fig. 3—Full-scale column testing system: (a) test setup; and (b) lever arm system for axial loading.

applied axial load. For a small lateral displacement, the true vertical load and the applied axial load can be considered approximately the same. On the other hand, the inclination of the applied axial force corresponding to Δ also has a horizontal component. Because this horizontal component is significant compared with the lateral load capacity of the column, it has to be subtracted from the horizontal actuator load to obtain the true lateral force applied to the column specimen.

Instrumentation

Load cells were used to monitor the applied forces. The lateral displacement at the application point of the lateral force was measured by a 500 mm stroke linear potentiometer. Seven pairs of linear potentiometers were mounted near the lower end of the column on the two faces perpendicular to the loading direction to measure the average curvatures. Electrical-resistance strain gages were mounted on the surfaces of the longitudinal and transverse reinforcing bars at selected positions in the column specimen, as depicted in Fig. 1.

Loading procedure

During testing, the axial load was maintained approximately constant, whereas the lateral force was cycled under lateral displacement control conditions. Three single cycles corresponding to an increment of 0.25% peak drift ratio Δ/L were initially applied. Three repetitive loading cycles were then applied for each of the peak drift ratios, Δ/L = 1, 1.5, 2, 3, 4, and 6%. For Specimen FHC1-0.2, an additional cycle at 8% drift was also attempted.

EXPERIMENTAL RESULTS

General observations

The six model columns developed stable responses to drift ratios ranging from 3 to 6% depending on the transverse reinforcement details and the axial load levels. Figure 4 illustrates the crack patterns for Column FHC1-0.2 at various loading stages. Flexural cracks perpendicular to the column axis formed first in the lower half of the column at drift ratios less than 0.5%. Some of the flexural cracks became inclined and extended into the web zone of the columns due to the influence of shear when the drift ratio increased to 1.0%. The highest lateral load-carrying capacity was typically recorded during the loading to approach the first peaks at a drift ratio of 2.0% for columns with an axial load ratio of 20 or at 1.5% for columns with an axial load ratio above 30%. At the same stage, the concrete cover crushed at the toes of the column. The spalling of the concrete cover gradually spread over the lower portion of the column with the increase of both the loading cycles and the drift displacement. Despite the concrete cover spalling, however, the confined core near the column end appeared to rotate in a stable manner, providing a satisfactory column performance until failure. The final failure of the columns was caused by longitudinal bar buckling and crushing of the confined concrete core. Columns FHC1-0.2 and FHC3-0.22 developed an ultimate peak drift ratio of 6.0% without serious degradation of their load-carrying capacity. The longitudinal bars of FHC1-0.2 buckled slightly when the column was pushed to a drift ratio of 8.0%. The column, however, was able to carry the full axial load and lateral force without significant degradation. The sudden buckling of the longitudinal bars caused failure of the column in the pull direction as evidenced by the sudden drop of lateral and axial loads. Column FHC3-0.2 failed similarly during the third loading cycle at a drift ratio of 6.0%. Other columns with lesser transverse reinforcement or higher axial load compared with these two columns failed at smaller drift ratios.

No rupture of reinforcement was observed in any of the tests. The buckling of longitudinal bars appeared to be significantly severed by the opening of the 90-degree anchorage of the cross ties, as shown in Fig. 5. This was consistent with the observations made by Xiao and Martirossyan.[9]

Although the concrete cover crushing initiated at the toes of the column, the most damaged zones appear to be in a portion approximately 200 to 300 mm above the critical section at the bottom of the column. This is likely due to the extra confinement provided to the column end by the footing, as observed by Bayrak and Sheikh.[6] As shown in Fig. 6, a closer examination of the tested specimens suggests the existence of a 45-degree triangular zone affected by the stub confinement. For this reason, it is suggested to consider a length of $0.5D$ as the zone affected by the footing confinement.

Hysteretic responses

Figure 7 to 9 show lateral shear force-drift ratio hysteretic relationships for the six full-scale HSC columns. The shear force values were obtained by subtracting the horizontal component of axial force from the applied lateral loads, for reasons discussed previously. The predicted flexural capacities V_{fACI} corresponding to an extreme concrete compressive strain of 0.003, as recommended by ACI 318-99,[7] and based on actual material strengths, are shown by dashed lines. The slopes of the dashed lines and the inclined solid line passing through the origin of the coordinates represent

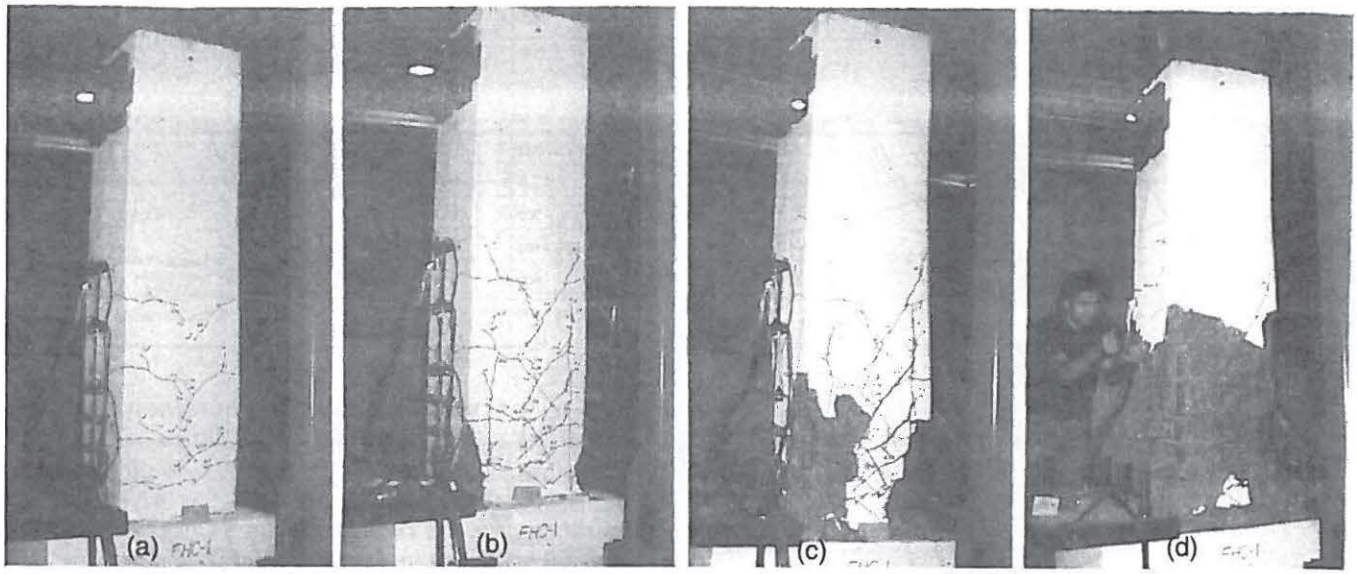

Fig. 4—Crack patterns of Column FHC1-0.2 at: (a) 1.0% drift ratio; (b) 2.0% drift ratio; (c) 6.0% drift ratio; and (d) failure.

the P-Δ effect. Symbols in Fig. 7 to 9 mark various loading stages where physical changes, such as concrete crushing or steel yielding, were observed.

The hysteretic behavior of the HSC columns appears to exhibit three stages: 1) the initial stage, characterized by a full participation of both confined core concrete and the unconfined cover concrete; 2) stable behavior with deformation contributed primarily by longitudinal steel yielding, cracking, and straining of confined core concrete; and 3) final failure. The termination of the initial stage and the beginning of the stable stage is typically marked by crushing and spalling of the unconfined cover concrete. The maximum lateral shear force-carrying capacity was achieved by the HSC columns immediately before crushing of the cover concrete. The maximum shear force and the corresponding drift ratio depend mainly on the axial load level, and were not significantly affected by the configuration of transverse reinforcement. As shown in Fig. 7 to 9, all columns developed and exceeded the flexural capacity calculated according to ACI 318-99.[7] Previous tests[4,10] have shown that the ACI code approach tends to overestimate the flexural strength of HSC columns failing in compression. All specimens tested in this study developed longitudinal bar yielding prior to concrete crushing, even Columns FHC2-0.34 and FHC4-0.33, both of which were predicted to exhibit compression failure based on the ACI code approach. Other reasons why the current study did not show similar trends of previous tests may include: 1) the loading condition differed from most previous tests where columns were tested under eccentric compression;[10] and 2) possible effects of full-scale versus smaller-scale specimens. The last point certainly deserves further study in the future.

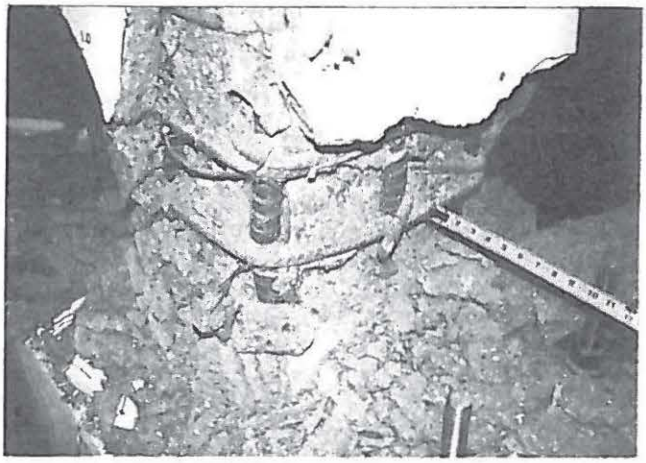

Fig. 5—Failure of 90-degree anchorage of cross-ties.

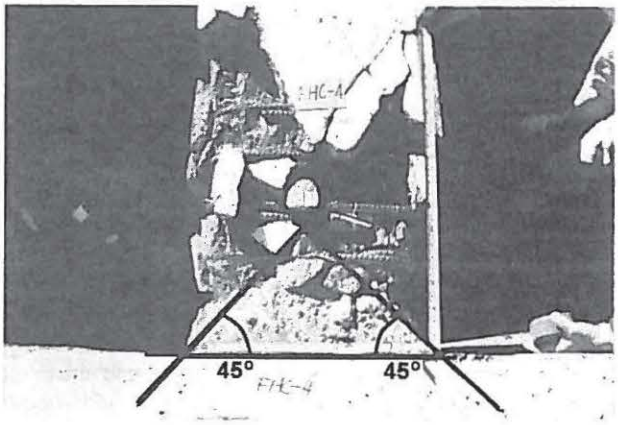

Fig. 6—Effect of stub on damage pattern in column.

Discussions on axial load effects

Model Column FHC1-0.2 developed a ductile response with the peak shear force above V_{fACI} until a drift ratio as large as 6.0% was reached, as shown in Fig. 7(a). Crushing of the concrete cover was noticed when load approached the first peak at $\Delta/L = 2.0$, where the maximum capacity was developed. The shape of the hysteresis loops for FHC1-0.2 after concrete cover spalling indicates a good energy dissipation capability. The column developed a capacity slightly less than V_{fACI} during the push loading at $\Delta/L = 8.0\%$. It then failed due to longitudinal bar buckling in the pull-loading direction. The initial response of Column FHC2-0.34 was stiffer than its counterpart, Model FHC1-0.20, as can be seen by comparing Fig. 7(a) and (b). The increased axial load, however, caused a significant reduction in the column deformability. Concrete

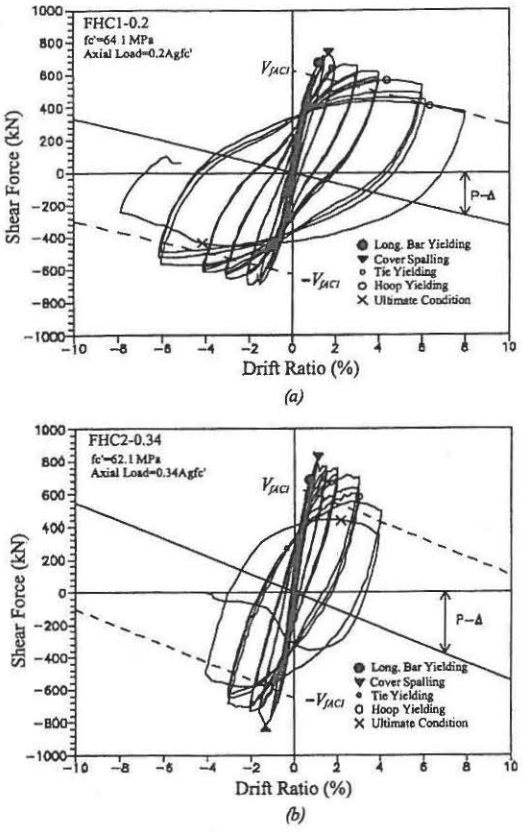

Fig. 7—Hysteresis loops of columns with 86% code-required transverse reinforcement: (a) FHC1-0.2; and (b) FHC2-0.34.

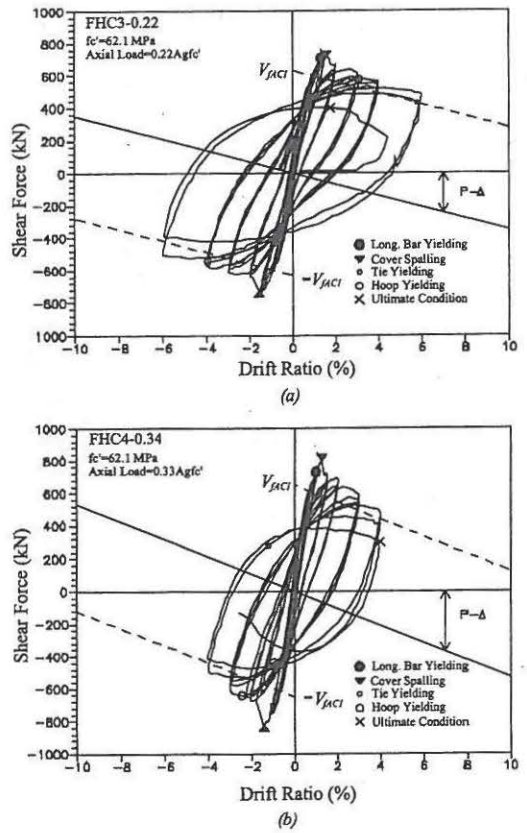

Fig. 8—Hysteresis loops of columns with 82% code-required transverse reinforcement: (a) FHC3-0.22; and (b) FHC4-0.33.

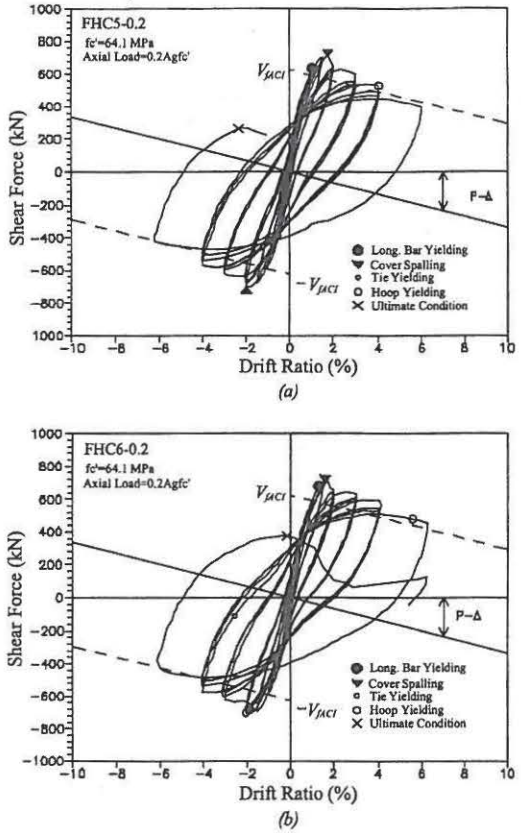

Fig. 9—Hysteresis loops of columns with different transverse reinforcement strength: (a) FHC5-0.2; and (b) FHC6-0.3.

cover crushed during loading to the first peak at $\Delta/L = 1.5\%$. Column FHC2-0.34 developed a stable response only up to a drift ratio of $\Delta/L = 3.0\%$, which was half of the ultimate drift ratio achieved by FHC1-0.20. Such a drastic degradation occurred during the loading cycle corresponding to a peak drift ratio of 4.0%. As shown in Fig. 7(b), however, the column was able to carry a shear force almost equal to the calculated flexural strength V_{fACI}. A comparison of Columns FHC1-0.20 and FHC2-0.34 also reveals that the increased axial load level results in a larger degradation of load-carrying capacity upon cycling of loading at a given peak drift ratio. Similar observations can be made for Specimens FHC3-0.22 and FHC4-0.33.

Effects of transverse steel strength

The transverse reinforcement spacing in the plastic hinge regions of model Columns FHC3-0.22 and FHC4-0.33 was 125 mm (5 in.), which was greater than that of FHC1-0.2 and FHC2-0.34. The transverse steel in FHC3-0.22 and FHC4-0.33, however, had a higher yield strength. As a consequence, the confinement index shown in Fig. 2 for FHC3-0.22 and FHC4-0.33 was close to the value for Columns FHC1-0.2 and FHC2-0.34. The hysteretic behaviors presented in Fig. 7 and 8 show that the counterpart model columns with identical values of confinement index and axial load ratio developed similar load-carrying capacities and ultimate drifts. Similarly, in comparison with the behavior of FHC5-0.2 shown in Fig. 9(a), an improved hysteretic behavior in terms of less severe degradation of capacity corresponding to the increase of drift ratio can be seen in Fig. 9(b) for Column FHC6-0.2.

Table 2—Column capacities

Specimen	${}_{ex}V_{1y}$, kN (${}_{ex}V_{1y}/{}_{an}V_{1y}$)	${}_{ex}V_{co}$, kN (${}_{ex}V_{co}/{}_{an}V_{co}$)	${}_{ex}V_{cc}$, kN (${}_{ex}V_{cc}/{}_{an}V_{cc}$)	Δ_{1y}/L, %	Δ_{co}/L, %	Δ_y/L, %	Δ_u/L, %
FHC1-0.2	701 (1.03)	755 (1.04)	751 (1.03)	1.25	1.60	1.34	7.30
FHC2-0.34	732 (1.09)	874 (1.15)	852 (1.11)	0.81	1.17	0.94	3.76
FHC3-0.22	670 (0.99)	783 (1.13)	723 (1.04)	1.25	1.55	1.35	5.80
FHC4-0.33	775 (1.13)	879 (1.16)	775 (1.02)	1.05	1.32	1.05	4.00
FHC5-0.2	658 (0.96)	769 (1.06)	715 (0.98)	1.04	1.83	1.13	5.00
FHC6-0.2	707 (1.03)	766 (1.05)	714 (0.98)	1.29	1.75	1.30	6.00

Note: Subscripts *ex* and *an* designate experimental and analytical values, respectively.

Effects of confinement index and spacing

The response of FHC5-0.2 was stable up to $\Delta/L = 3.0\%$ despite a drop of shear force during loading to achieve the first peak at $\Delta/L = 2.0\%$ due to the concrete cover spalling. As shown in Fig. 9(a), the degradation of peak shear force of FHC5-0.2 upon cycling of load becomes apparent for $\Delta/L \geq 3.0\%$. The peak shear force reduced below V_{fACI} after the first cycle at $\Delta/L = 3.0\%$, particularly in the push-loading direction. The column failed after completing one cycle of loading at $\Delta/L = 6.0\%$. This column can also be considered as the counterpart model of Columns FHC1-0.2 and FHC3-0.22 for exhibiting the effects of wider transverse reinforcement spacing, and, thus, a smaller confinement index. Apparently, the increasing in hoop spacing or reduction in confinement index led to a decrease in the maximum drift achieved.

ANALYSIS OF COLUMN CAPACITIES

To characterize the response of the full-scale model columns, the lateral load-carrying capacity and the deformation corresponding to distinct physical changes need to be defined and discussed. Figure 10 schematically depicts the monotonic shear force displacement relationship with the points marked for major physical changes along with a bilinear idealized behavior.

Flexural cracking is the first noticeable phenomenon observed for the columns. Cracking is less important for seismic design, however, since most reinforced concrete columns are expected to perform in the postcracking stage when subjected to seismic loading. The more meaningful physical change is the first yield of the longitudinal reinforcement for columns with axial load below the balanced axial load. In Fig. 10, the shear force and the deformation corresponding to first yield of longitudinal reinforcement are denoted as V_{1y} and Δ_{1y}, respectively. The first yield can be determined in the column specimens based on strain measurement of longitudinal bars. As shown in Fig. 10, a drop of load-carrying capacity typically accompanied the concrete cover crushing. For the model columns tested, the shear force at concrete cover crushing V_{co} was also the recorded maximum load-carrying capacity. A ductile response of the reinforced concrete column relies mainly on the inelastic deformation of the longitudinal reinforcement and the confined concrete core. Thus, assessing the capacity of the column after cover concrete spalling is of particular importance. The peak capacity based on the confined concrete core after cover spalling is defined as V_{cc}. The capacity at the ultimate failure V_u is defined as 90% of V_{cc} in this study. This definition was based on the observation that beyond this stage, the load-carrying capacity of the specimens becomes unstable.

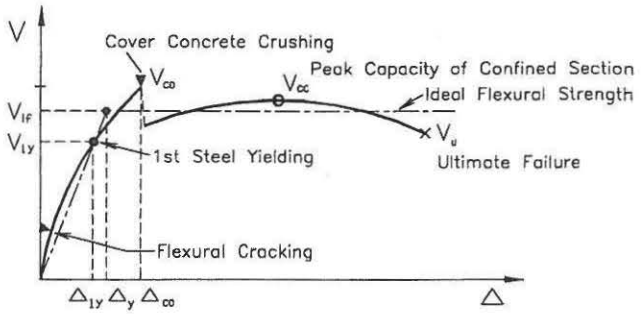

Fig. 10—Definitions of characteristic capacities and displacements.

Since the column response is not purely elastoplastic, a bilinear behavior should be defined to provide the ductility index for the model columns. In Fig. 10, the bilinear idealization is expressed by the linked lines with a stiffness corresponding to the secant stiffness at first yield of longitudinal bars and an ideal flexural capacity V_{if}. The yield displacement is then given as

$$\Delta_y = \frac{V_{if}}{V_{1y}}\Delta_{1y} \tag{3}$$

Thus, the displacement ductility factor can be defined as

$$\mu_\Delta = \frac{\Delta}{\Delta_y} \tag{4}$$

For the six model columns, the flexural strength based on confined core V_{cc} is used as V_{if} because the peak shear forces after the spalling of cover concrete and prior to failure were relatively stable.

The values of the previously mentioned characteristic parameters, obtained from the test results of the six full-scale model columns, are shown in Table 2. Note that the P-Δ effects have been considered for all the capacity values. In Table 2, the experimental capacity values are also compared with analytical capacities in parentheses. The calculated capacities were based on moment-curvature analysis of the column critical section using the stress-strain relationship of confined HSC proposed by Martirossyan.[11] Following the same definition described previously, the capacities at first yield V_{1y} and at concrete cover crushing V_{co} were analyzed using the actual material properties and an ultimate compressive strain of 0.005 for unconfined HSC. The analysis for ideal capacity V_{if} was based on an extreme compressive strain of 0.005 for confined concrete. As shown in Table 2, the analysis provides

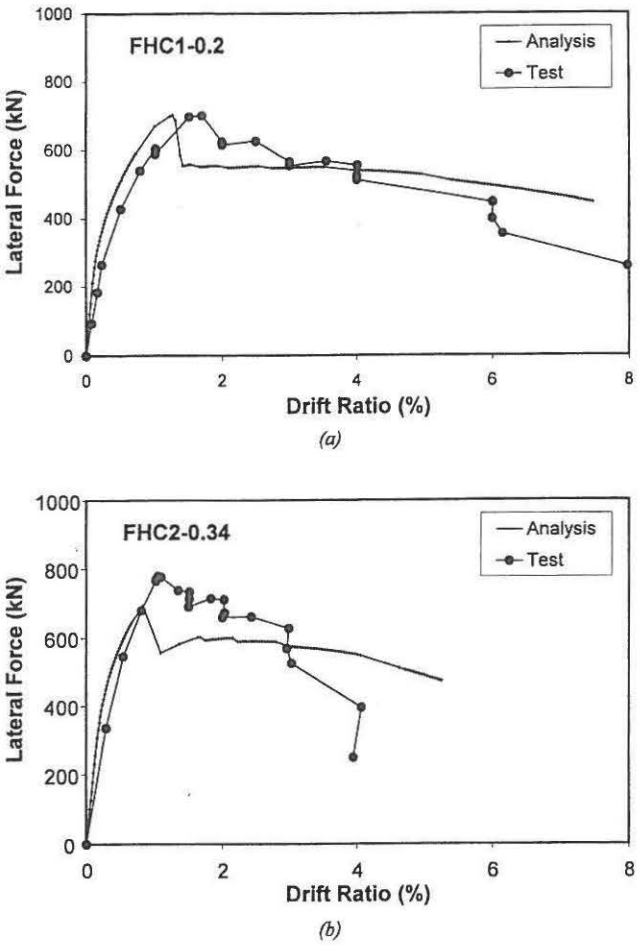

Fig. 11—Comparisons of pushover analysis and test results for: (a) Specimen FHC1-0.2; and (b) FHC2-0.34.

reasonably close estimations to the test results of the capacities corresponding to the first yield of longitudinal reinforcement and the capacities based on the confined core after cover concrete spalling. The analytical results underestimated the test results of the capacities corresponding to the cover concrete crushing.

A pushover analysis based on moment-curvature analysis was also attempted to capture the main features of the mechanical behavior of the HSC column specimens. The analytical approach was modified from a method developed in previous studies.[11,12] The column was modeled as a beam element with a hinge at its end. The moment-rotation characteristics of the hinge were defined based on a moment-curvature analysis. In the analysis, the cover concrete was analyzed as unconfined concrete, while the concrete inside the transverse reinforcement is assumed to be confined concrete. Stress-strain relationships of HSC proposed by Martirossyan[11] were used in the analysis. A length equal to half of the column section depth was subtracted from the original column length to account for the effect of stub footing confinement, as discussed previously. Other details of the analysis can be found in previous studies.[11,12] Figure 11(a) and (b) show the pushover analytical results compared with the envelopes from the tests of Specimens FHC1-0.2 and FHC2-0.34. For Specimen FHC1-0.2, the analysis provides a very close estimate to the maximum load-carrying capacity. It slightly underestimates the behavior after the crushing of cover concrete, however. The pushover analysis underestimates the response of Specimen FHC2-0.34 before failure at a drift ratio of 4%. Overall, the simple pushover analysis gives a reasonable description of the behavior of the test specimens.

CONCLUSIONS

The main findings from the test results of the full-scale model HSC columns subjected to a constant axial load and cyclic lateral forces can be summarized as follows.

1. The hysteretic behavior of the HSC columns can be characterized by three distinct stages: 1) the initial stage with the full participation of both confined core concrete and unconfined cover concrete; 2) stable behavior with deformation contributed primarily by longitudinal steel yielding and straining of confined core concrete; and 3) final failure;

2. The termination of the initial stage, or the beginning of the stable stage, is marked by the crushing and spalling of unconfined cover concrete. The maximum lateral shear force-carrying capacity is typically achieved by the HSC columns tested in the program at the crushing of cover concrete. The maximum shear force and the corresponding drift ratio depend mainly on the concrete section properties, including the axial load levels, and are not significantly affected by the configuration of transverse reinforcement;

3. The stable behavior after concrete cover spalling, which is most important for seismic design, was significantly affected by both the level of axial load and the details of transverse reinforcement. Model columns reinforced with transverse reinforcement of more than 82% of the ACI 318-99 requirement developed ductile response with an ultimate drift ratio of 6.0% when the axial load was $0.2A_g f_c'$. The ultimate drift ratios decreased for model columns with less transverse reinforcement or higher axial load levels;

4. The failure of all of the model columns was dominated by the buckling of longitudinal reinforcement, followed by the total crushing of core concrete. The failure might have been initiated, or at least compounded, by the opening of the 90-degree anchorage of the cross-ties;

5. The use of higher-strength transverse reinforcement was found to be effective in providing additional confinement and ductility. In particular, increased transverse steel strength can effectively offset the negative effects due to widening of hoop spacing;

6. Analysis based on the equivalent compressive stress block corresponding to an ultimate concrete compressive strain of 0.003, as recommended by ACI 318-99, provides a predictable but conservative estimate to the flexural strength of the HSC full-scale column models tested in this study. The analysis based on a proposed stress-strain model for confined HSC can estimate the characteristic capacity values corresponding to major physical changes reasonably well;

7. Though the specimens were all substandard compared with the current ACI 318 code requirements for transverse reinforcement in the potential plastic hinge regions of a column, the test results show that the current code provision appeared to be overconservative for lower axial load levels, but less conservative for higher axial load levels; and

8. The available analytical model based on moment-curvature analysis was shown to be capable of predicting the force-deformation response of the columns.

ACKNOWLEDGMENTS

The research described in this paper has been funded by Carpenters/Contractors Cooperation Committee (CCCC), Inc. through collaboration with ESI Inc. The research project also received supports from Concrete Reinforcing Steel Institute (CRSI), Fontana Steel, Inc., and Transit Mixed Concrete Corp. Cooperation from M. Pourzanjani and Roger Y. Li of ESI are warmly appreciated. The authors would like to thank H. Wu and A. Esmaeily-Ghasemabadi, graduate research assistants at the University of Southern California, for their help during testing.

NOTATION

A_{ch}	=	cross-sectional area of column measured out-to-out of transverse reinforcement
A_g	=	gross area of column section
A_{sh}	=	total transverse steel cross-sectional area within spacing s
f_c'	=	specified compressive strength of concrete
f_{yh}	=	specified yield strength of transverse reinforcement
h_c	=	cross-sectional dimension of column core measured center-to-center of outermost peripheral hoops
L	=	column height
V	=	column shear force
V_{1y}	=	column capacity at first yield of reinforcement
V_{cc}	=	column capacity based on confined section
V_{co}	=	column capacity at unconfined cover crushing
V_{fACI}	=	flexural strength based on ACI code recommendation
V_{if}	=	ideal flexural strength
V_u	=	column capacity at ultimate failure
$\Delta_{1y}, \Delta_y, \Delta_{co}, \Delta_u$	=	column displacements corresponding to V_{1y}, V_{if}, V_{co}, and V_u
μ_Δ	=	displacement ductility

REFERENCES

1. Hester, W. T., ed., *High-Strength Concrete*, Second International Symposium, SP-121, American Concrete Institute, Farmington Hills, Mich., 1990, 786 pp.

2. Li, B., and Park, R., "Strength and Ductility of Reinforced Concrete and Frames Constructed Using High-Strength Concrete," *Research Report* 94-5, Department of Civil Engineering, University of Canterbury, New Zealand, 1994, 389 pp.

3. Malhotra, V. M., ed., *High-Performance Concrete*, Proceedings, ACI International Conference, Singapore, SP-149, American Concrete Institute, Farmington Hills, Mich., 1994, 844 pp.

4. ACI-ASCE Committee 441, "High-Strength Concrete Columns: State of the Art," *ACI Structural Journal*, V. 94, No. 3, May-June 1997, pp. 323-335.

5. Xiao, Y., and Martirossyan, A., "Seismic Performance of High-Strength Concrete Columns," *ASCE Journal of Structural Engineering*, V. 124, No. 3, Mar. 1998, pp. 241-251.

6. Bayrak, O., and Sheikh, S. S., "Confinement Reinforcement Design Considerations for Ductile HSC Columns," *ASCE Journal of Structural Engineering*, V. 124, No. 9, Sept. 1998, pp. 999-1010.

7. ACI Committee 318, "Building Code Requirements for Reinforced Concrete (ACI 318-99) and Commentary (318R-99)," American Concrete Institute, Farmington Hills, Mich., 1999, 391 pp.

8. Anderson, J. C.; Xiao, Y.; and Yin, Z., "High-Strength Concrete Using Local Materials in Southern California," Center for Research in Earthquake and Construction Engineering (CRECE), Department of Civil Engineering, University of Southern California, Sept. 15, 1994, 107 pp.

9. Xiao, Y., and Martirossyan, A., "Eccentric Compression Testing of High-Strength Concrete Columns," *Report* No. USC-SERP-96/02, Structural Engineering Research Project, Department of Civil Engineering, University of Southern California, 1996, 40 pp.

10. Ibrahim, H. H. H., and MacGregor, J. G., "Modification of the ACI Rectangular Stress Block for High-Strength Concrete," *ACI Structural Journal*, V. 94, No. 1, Jan.-Feb. 1997, pp. 40-48.

11. Martirossyan, A., "Performance of Reinforced High-Strength Concrete Columns," PhD thesis, *Report* No. USC-SERP-98/06, Structural Engineering Research Project, Department of Civil Engineering, University of Southern California, 1998, 377 pp.

12. Xiao, Y., and Ma, R., "Seismic Behavior of High-Strength Concrete Beams," *The International Journal of the Structural Design of Tall Buildings*, V. 7, No. 1, Mar. 1998, pp. 73-90.

13. Sheikh, S. A., and Khoury, S. S., "A Performance-Based Approach for the Design of Confining Steel in Tied Columns," *ACI Structural Journal*, V. 94, No. 4, July-Aug. 1997, pp. 421-431.